6th IEEE RAS/EMBS International Conference on
Biomedical Robotics and Biomechatronics (BioRob)
June 26-29, 2016. UTown, Singapore

Disturbance Observer-Based Motion Control of Paramagnetic Microparticles Against Time-Varying Flow Rates

Hazem Abass*†, Mostafa Shoukry*†, Anke Klingner*,
Abdelrahman Hosney*, Sarthak Misra‡§, and Islam S. M. Khalil*

***Abstract*— We control the motion of paramagnetic microparticles with average diameter of 100 μm inside microfluidic channels against and along time-varying flow rates. The drag force and the force due to time-varying flow rate are modeled as time-varying disturbance force. This force is estimated using a disturbance force observer and compensated using a magnetic-based closed-loop control system. The closed-loop control with disturbance compensation decreases the steady-state error by 81.4%, 70.2%, and 70.3% at flow rates of 6 ml.hr^{-1}, 17 ml.hr^{-1}, and 35 ml.hr^{-1}, respectively. The proposed control system is essential to translate these paramagnetic microparticles and magnetic drug carriers into *in vivo* applications.**

I. INTRODUCTION

Translation of targeted therapy using magnetic microrobotic systems into *in vivo* applications remains a challenge because of many major technological barriers. One of these barriers is the ability to provide sufficient magnetic force and magnetic torque to drive (and hold) and steer these microrobotic systems against and along the flowing streams of body fluids [1]-[8]. Sanchez *et al.* have demonstrated that self-propelled microjets can provide enough propulsive force to overcome forces due to drag and time-varying flow rates [9]. The targeting accuracy of these microjets has been improved by using magnetic-based closed-loop control system and microscopic guidance [10]. However, the dependence of the locomotion mechanism of microjets on the catalytic decomposition of hydrogen peroxide solution into water and oxygen does not make them suitable for biological applications. Nacev *et al.* [11] have demonstrated the localization of ferromagnetic nanoparticles inside rats using external magnetic field without feedback closed-loop control. Recently, Khalil *et al.* have presented a magnetic-based closed-loop control system that consists of an inner- and outer-loops [12], [13]. The inner-loop (positive feedback) estimates and compensates the disturbance force exerted on a microrobotic agent, whereas the outer-loop (negative feedback) achieves stability of the control system. In this paper, we implement the control systems of [12], which have not been implemented experimentally in the presence of time-varying flow rates inside microfluidic channels. First, we model the motion of paramagnetic microparticles inside channels with time-varying flow and develop an electromagnetic system (Fig. 1) that enables control of microparticles against maximum flow rate of 35 ml.hr^{-1}. This flow rate is similar to that used in animal experimentation. Mouse carotid flow rates average approximately between 14.4 ml.hr^{-1} to 42 ml.hr^{-1} [11]. Second, we use the model of the microparticles and electromagnetic system in the design of a disturbance force observer [14]-[16] to reject the estimated disturbance forces due to drag and time-varying flow.

The remainder of this paper is organized as follows: Section II provides a mathematical model for the paramagnetic microparticles inside channels with time-varying flow rates.

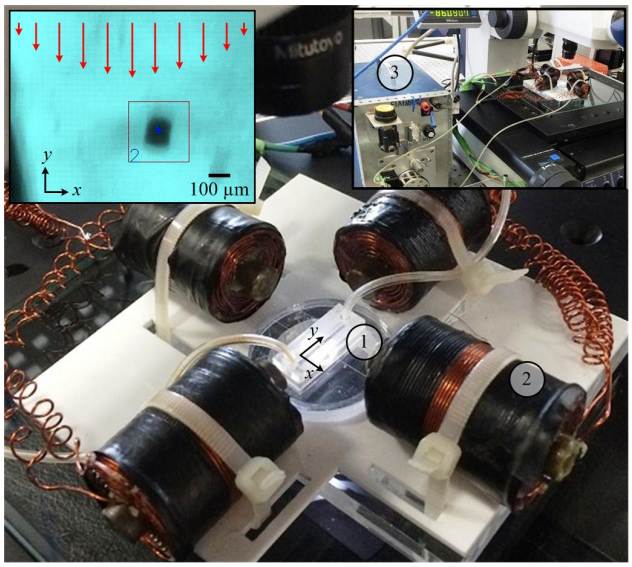

Fig. 1. An electromagnetic system with 4 orthogonal electromagnetic coils that surround a microfluidic channel ①. Paramagnetic microparticle is contained inside the channel and controlled against and along the flowing streams (flow along y-axis) of a fluid (top-right inset). This electromagnetic configuration ② enables motion control against time-varying flow rates. The flow rate is controlled using a dual pump ③ (FIAlab-3200 Dual Pump Sequential Injection Analyzer, FIAlab Instruments Inc., Bellevue, USA). The electromagnetic coils can overcome maximum flow rate of 35 ml.hr^{-1} using maximum magnetic field gradient of 220 mT.m^{-1}. The red arrows indicate the direction of the flow inside the channel (top-left corner).

This work was supported by funds from the German University in Cairo and the DAAD-BMBF funding project. The authors also acknowledge the funding from the Science and Technology Development Fund in Egypt (No. 23016).

*The authors are affiliated with the German University in Cairo, New Cairo City 11835, Egypt.

†The authors assert equal contribution and joint first authorship

‡Department of Biomechanical Engineering, MIRA–Institute for Biomedical Technology and Technical Medicine, University of Twente, Enschede, The Netherlands.

§Department of Biomedical Engineering, University of Groningen and University Medical Centre Groningen, The Netherlands.

Point-to-point motion control experiments of microparticles against flow rates of 4 ml.hr^{-1}, 6 ml.hr^{-1}, 17 ml.hr^{-1}, and 35 ml.hr^{-1}, are included in Section III. In addition, we compare the motion control characteristics of the microparticle for closed-loop control systems with and without disturbance compensation. Finally, Section IV concludes and provides directions for future work.

II. MODELING AND MOTION CONTROL OF MICROPARTICLES INSIDE CHANNELS

The motion of a paramagnetic microparticle under the influence of a magnetic field ($\mathbf{B}(\mathbf{P})$), and in a fluid (with volume V) with time-varying flow rate $\left(Q(t) = \frac{\mathrm{d}V}{\mathrm{d}t}\right)$ is modeled [17]. This model is used in the design of a motion control system to localize the microparticles against time-varying flow rates.

A. Modeling of the Microparticles Inside Channels

The governing equation of a microparticle inside fluidic channel with flow is given by

$$\mathbf{F}_{\mathrm{B}}(\mathbf{P}) + \mathbf{F}_{\mathrm{Q}}(\mathbf{P}) + \mathbf{F}_{\mathrm{d}}(\dot{\mathbf{P}}) = 0, \tag{1}$$

where $\mathbf{F}_{\mathrm{B}}(\mathbf{P}) \in \mathbb{R}^{3\times1}$ is the magnetic force at point ($\mathbf{P} \in \mathbb{R}^{3\times1}$), $\mathbf{F}_{\mathrm{Q}}(\mathbf{P}) \in \mathbb{R}^{3\times1}$ is the force due to time-varying flow rate, and $\mathbf{F}_{\mathrm{d}}(\dot{\mathbf{P}}) \in \mathbb{R}^{3\times1}$ is the drag force on the microparticle. We consider the second and third terms in (1) as disturbance force ($\mathbf{d}(\mathbf{P})$) that is given by

$$\mathbf{d}(\mathbf{P}) = \mathbf{F}_{\mathrm{Q}}(\mathbf{P}) + \mathbf{F}_{\mathrm{d}}(\dot{\mathbf{P}}). \tag{2}$$

Our aim is to compensate this force by the magnetic force exerted on the microparticle using an orthogonal configuration of electromagnetic coils (Fig. 1). This magnetic force is given by [18]

$$\mathbf{F}_{\mathrm{B}}(\mathbf{P}) = (\mathbf{m}\cdot\nabla)\mathbf{B}(\mathbf{P}) = (\mathbf{m}\cdot\nabla)\widetilde{\mathbf{B}}(\mathbf{P})\mathbf{I} = \mathbf{\Lambda}(\mathbf{m},\mathbf{P})\mathbf{I}, \tag{3}$$

where $\mathbf{m} \in \mathbb{R}^{3\times1}$ and $\mathbf{B}(\mathbf{P}) \in \mathbb{R}^{3\times1}$ are the magnetic dipole moment of the microparticle and the induced magnetic field, respectively. Further, $\widetilde{\mathbf{B}}(\mathbf{P}) \in \mathbb{R}^{3\times4}$ and $\mathbf{I} \in \mathbb{R}^{4\times1}$ are the magnetic field-current map and the input current to the four electromagnetic coils, respectively. Furthermore, $\mathbf{\Lambda}(\mathbf{m},\mathbf{P}) \in \mathbb{R}^{4\times3}$ is the magnetic force-current map. The largest microparticle we use in this study is less than 100 μm in diameter, and the maximum magnetic field gradient exerted on its dipole moment is 220 mT.mm^{-1} (maximum speed of the microparticle is 375 μm.s^{-1}). Laminar flow condition is justified as the Reynolds number $\left(Re = \frac{\rho Q}{l\eta}\right)$ is calculated to be less than 0.1, for the density (ρ) of the fluid (900 kg.m^{-3} for oil [19]), maximum flow rate of 35 ml.hr^{-1}, viscosity (η) of the oil is 50 mPa.s, and channel side-length (l) of 1.5 mm. Therefore, we can assume laminar flow condition and the fluid velocity vector ($\mathbf{v}(\mathbf{P})$) depends on the position as follows [20]:

$$\mathbf{v}(\mathbf{P}) = -\frac{2Q}{A}\left(1 - \frac{4x^2}{w^2}\right)\hat{\mathbf{y}}, \tag{4}$$

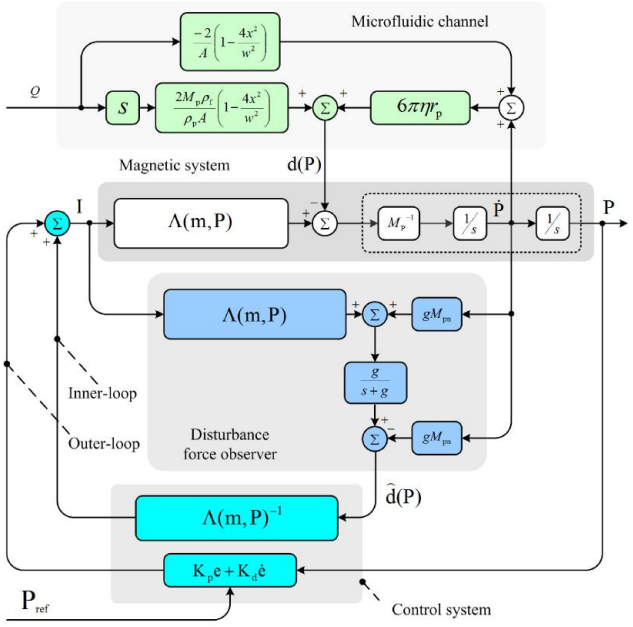

Fig. 2. The control architecture of the microparticle against or along time-varying flow (Q) inside microfluidic channel with width w. The velocity of the microparticle ($\dot{\mathbf{P}}$) and the input current ($\mathbf{I}$) to the electromagnetic coils are used to estimate the disturbance force ($\mathbf{d}(\mathbf{P})$) exerted on the microparticle. The disturbance observer represents a positive inner-loop in the control system that estimates ($\widehat{\mathbf{d}}(\mathbf{P})$) and rejects the disturbance force. The outer-loop of the control system stabilizes the motion of the microparticle within the vicinity of the reference position ($\mathbf{P}_{\mathrm{ref}}$). M_{p} and M_{pn} are the mass and nominal mass of the microparticle, respectively. The proportional- and derivative-gain matrices ($\mathbf{K}_{\mathrm{p}}$ and $\mathbf{K}_{\mathrm{d}}$) and the the corner frequency (g) must be positive-definite and positive, respectively.

where x is the x-component of the position vector ($\mathbf{P}$) from the center of the channel and the flow rate (Q) is applied along negative $\hat{\mathbf{y}}$-direction, where $\hat{\mathbf{y}}$ is a unit-vector (opposite to the direction of the flow). Furthermore, A is the cross-sectional area of the channel. In our experimental setup, the cross-sectional area of the microfluidic channel is rectangular with height (h) and width (w) of 1.5 mm and 2 mm, respectively. A time-varying flow rate results in a force due to acceleration of the fluid that is given by

$$\mathbf{F}_{\mathrm{Q}}(\mathbf{P}) = M_{\mathrm{p}}\frac{\rho_{\mathrm{f}}}{\rho_{\mathrm{p}}}\frac{\mathrm{d}\mathbf{v}(\mathbf{P})}{\mathrm{d}t} = -\frac{2M_{\mathrm{p}}\rho_{\mathrm{f}}\dot{Q}}{\rho_{\mathrm{p}}A}\left(1 - \frac{4x^2}{w^2}\right)\hat{\mathbf{y}}. \tag{5}$$

In (5), M_{p} and $\dot{Q}$ are the mass of the magnetic microparticle and the time-derivative of flow rate ($\dot{Q} = \frac{\mathrm{d}Q}{\mathrm{d}t}$). Further, ρ_{f} and ρ_{p} are the density of the fluid and the microparticle, respectively. The drag force is given by the following Stokes law since we assume laminar flow:

$$\mathbf{F}_{\mathrm{d}}(\dot{\mathbf{P}}) = 6\pi\eta r_{\mathrm{p}}\left(\mathbf{v}(\mathbf{P}) + \dot{\mathbf{P}}\right), \tag{6}$$

where η is the dynamic viscosity of the fluid and r_{p} is the radius of the microparticle. Further, $\dot{\mathbf{P}}$ and $\mathbf{v}(\mathbf{P})$ are the velocity vectors of the microparticle and the fluid with respect to a reference frame, respectively. We rewrite (1)

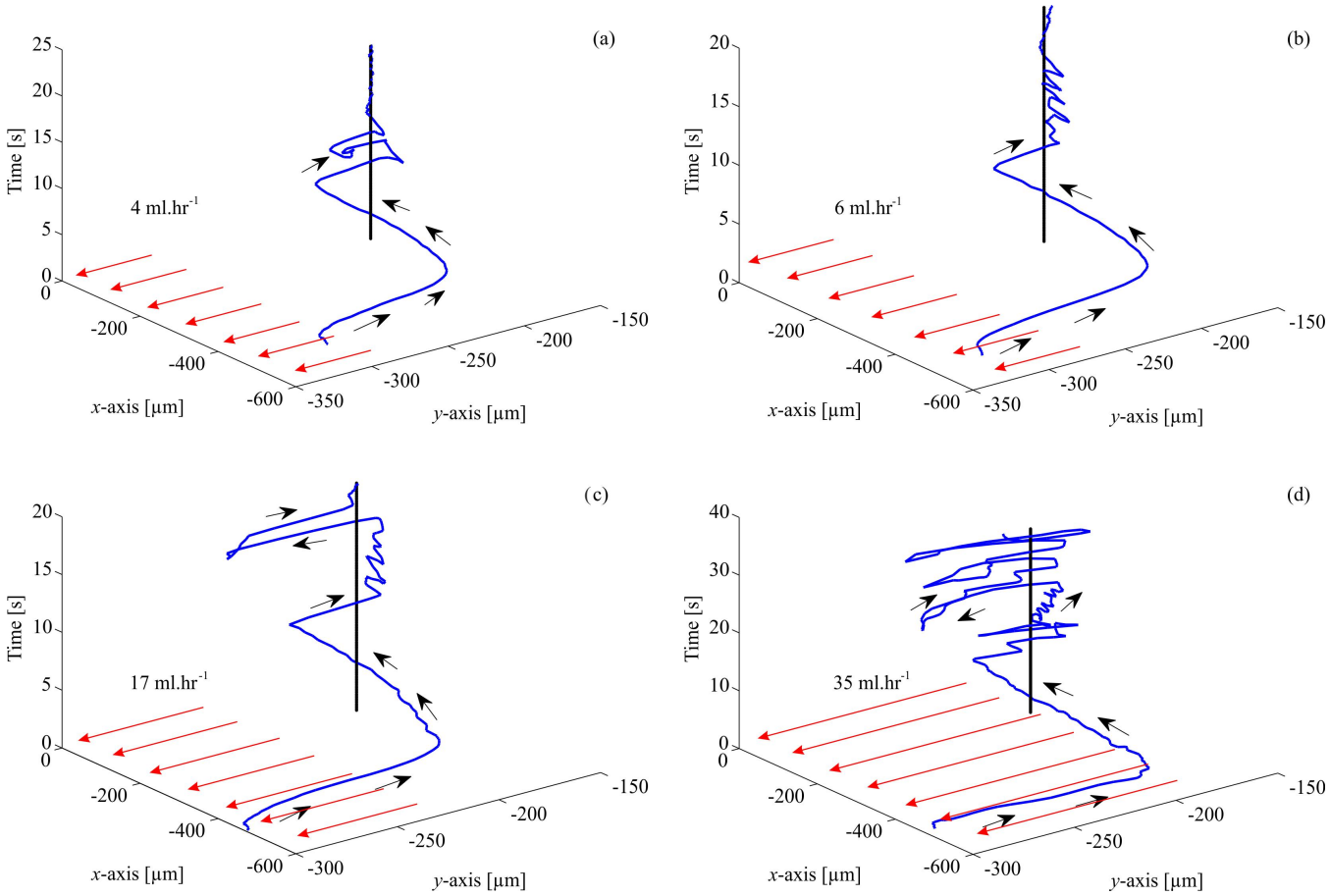

Fig. 3. A representative motion control result of a microparticle against flow rates of 4 ml.hr^{-1}, 6 ml.hr^{-1}, 17 ml.hr^{-1}, and 35 ml.hr^{-1} using control law (9). (a, b, c, and d) At flow rates of 4 ml.hr^{-1}, 6 ml.hr^{-1}, 17 ml.hr^{-1}, and 35 ml.hr^{-1}, their respective average speed and maximum steady-state error of the controlled microparticle are 150 μm.s^{-1} and 10 μm, 145 μm.s^{-1} and 47 μm, 135 μm.s^{-1} and 55 μm, and 125 μm.s^{-1} and 64 μm. The red lines indicate the time-varying flow inside the channel, whereas the black arrows represent the direction of the microparticle. *Please refer to the accompanying video that demonstrates the motion control of a microparticles against different flow rates using a PD control system.*

using (3), (4) and (5) to obtain

$$\dot{\mathbf{P}} = \frac{\mathbf{\Lambda}(\mathbf{m},\mathbf{P})\mathbf{I}}{6\pi\eta r_{\mathrm{p}}} - \frac{2}{A}\left[\frac{M_{\mathrm{p}}\dot{Q}\rho_{\mathrm{f}}}{6\pi\eta r_{\mathrm{p}}\rho_{\mathrm{p}}} + Q\right]\left(1 - \frac{4x^2}{w^2}\right)\hat{\mathbf{y}}. \quad (7)$$

A block diagram representation of the model of the microparticles inside the microfluidic channel is shown in Fig. 2. We use the model of the microparticle in the design of a robust motion control system based on disturbance estimation and compensation.

B. Design of a Robust Motion Control System

The microparticle is subjected to drag force (5) and force due to the time-varying flow (6). These forces are estimated using the following disturbance force observer [21]:

$$\widehat{\mathbf{d}}(\mathbf{P}) = \frac{g}{s+g}\left(\mathbf{F}_{\mathrm{Bn}}(\mathbf{P}) + gM_{\mathrm{pn}}\dot{\mathbf{P}}\right) - gM_{\mathrm{pn}}\dot{\mathbf{P}}, \quad (8)$$

where $\widehat{\mathbf{d}}(\mathbf{P})$ is the estimate of the disturbance force ($\mathbf{d}(\dot{\mathbf{P}})$). Further, $\mathbf{F}_{\mathrm{Bn}}(\mathbf{P})$ and M_{pn} are the nominal magnetic force and the nominal mass of the microparticle, respectively. The disturbance force is estimated through a low-pass filter ($\frac{g}{s+g}$) with a corner frequency g. This corner frequency can be increased to decrease the convergence time of the estimated disturbance to the actual disturbance force. However, measurement noise could limit the value of the corner frequency. We devise a proportional-derivative (PD) control system with disturbance compensation [22], [23]

$$\mathbf{F}_{\mathrm{B}}(\mathbf{P}) = -\widehat{\mathbf{d}}(\dot{\mathbf{P}}) + \mathbf{K}_{\mathrm{p}}\mathbf{e} + \mathbf{K}_{\mathrm{d}}\dot{\mathbf{e}}. \quad (9)$$

In (9), $\mathbf{e}$ and $\dot{\mathbf{e}}$ are the position and velocity tracking errors, respectively. Further, $\mathbf{K}_{\mathrm{p}}$ and $\mathbf{K}_{\mathrm{d}}$ are the proportional- and derivative-gain matrices, respectively. Implementation of the control system (9) is represented in Fig. 2. The first term in (9) represents an inner-loop that estimates the drag force and force due time-varying flow and rejects their effect. This inner-loop provides positive-feedback to the control system and cannot achieve stability. The second and third terms in (9) provide an outer-loop to achieve stability. We assume that the inner-loop achieves perfect cancelation of the disturbance forces. Therefore, the error dynamics of the control system is approximated using

$$\dot{\mathbf{e}} + \mathbf{K}_{\mathrm{d}}^{-1}\mathbf{K}_{\mathrm{p}}\mathbf{e} = 0. \quad (10)$$

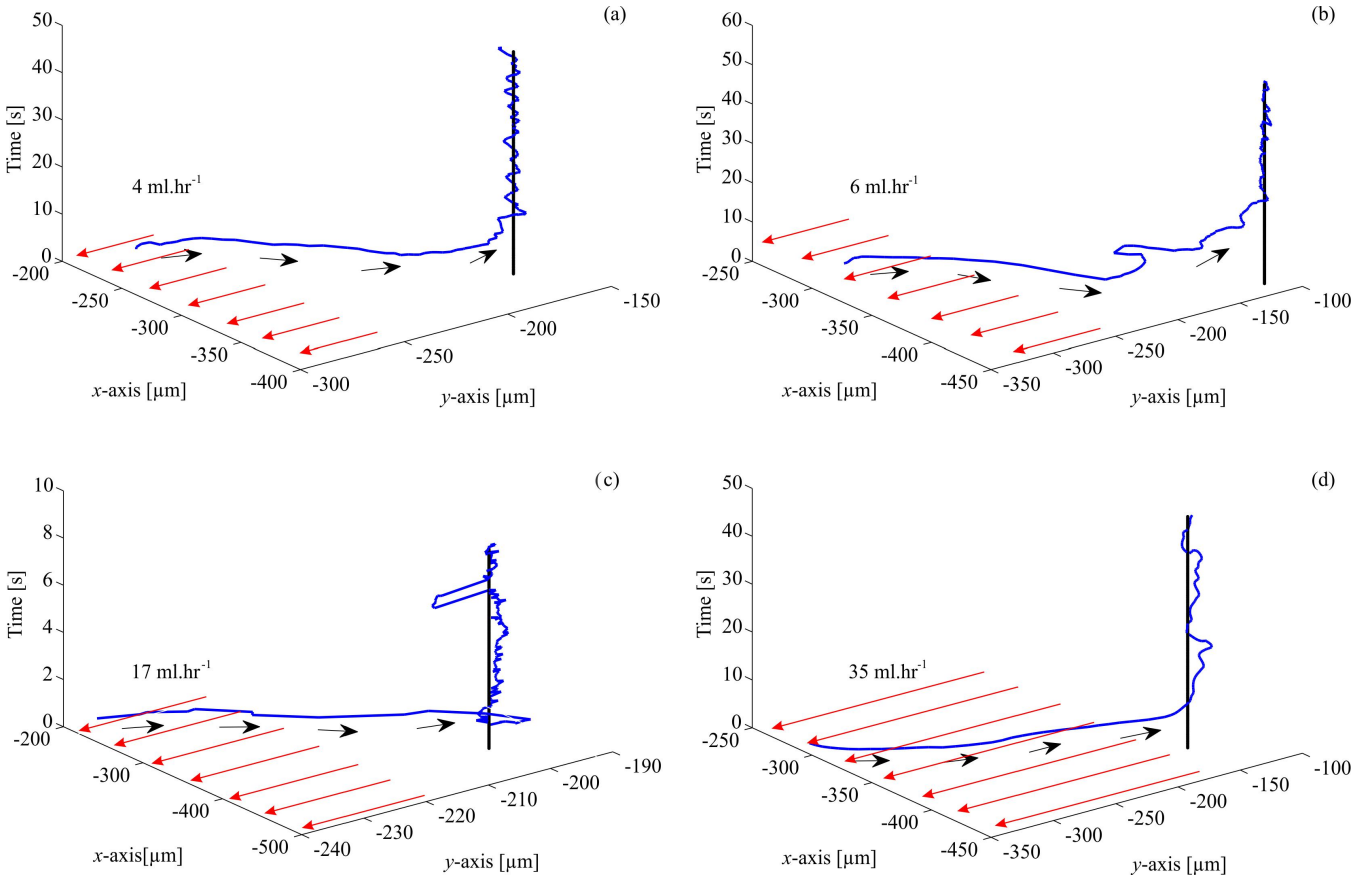

Fig. 4. A representative motion control result of a microparticle against flow rates of 4 ml.hr^{-1}, 6 ml.hr^{-1}, 17 ml.hr^{-1}, and 35 ml.hr^{-1} using control law (9). (a, b, c, and d) At flow rates of 4 ml.hr^{-1}, 6 ml.hr^{-1}, 17 ml.hr^{-1}, and 35 ml.hr^{-1}, their respective average speed and maximum steady-state error of the controlled microparticle are 300 μm/s and 5 μm, 322 μm.s^{-1} and 14 μm, 350 μm.s^{-1} and 15 μm, and 370 μm.s^{-1} and 64 μm. The red lines indicate the time-varying flow inside the channel, whereas the black arrows represent the direction of the microparticle. *Please refer to the accompanying video that demonstrates the motion control of a microparticles against different flow rates using a PD control system with disturbance compensation.*

The error dynamics (10) indicates that the matrix $\mathbf{K}_{\mathrm{d}}^{-1}\mathbf{K}_{\mathrm{p}}$ must be positive-definite to achieve stable position tracking error. In (10), the position and velocity tracking errors are give by

$$\mathbf{e} = \mathbf{P} - \mathbf{P}_{\mathrm{ref}} \quad \text{and} \quad \dot{\mathbf{e}} = \dot{\mathbf{P}}, \tag{11}$$

where $\mathbf{P}_{\mathrm{ref}}$ is a fixed reference position. Control law (9) is implemented on an electromagnetic system and controlled time-varying flow rate with and without disturbance compensation.

III. CONTROL OF MICROPARTICLES AGAINST TIME-VARYING FLOW RATES

Our motion control experimental results are done using an electromagnetic system with closed-configuration (Fig. 1). This system generates maximum magnetic field and field gradient of 65 mT and 220 mT.mm^{-1}, respectively. A microfluidic channel (width and depth of 1.5 mm and 2 mm, respectively) is mounted in the common center of the electromagnetic configuration. The channel is connected to a dual pump (FIAlab-3200 Dual Pump Sequential Injection Analyzer, FIAlab Instruments Inc., Bellevue, USA) to provide time-varying flow rates. Motion of the microparticles is tracked using a microscopic system (Stemi 2000-C, Carl Zeiss Microscopy, LLC, New York, U.S.A) and our feature tracking algorithm [21]. The microparticles (PLAParticles-M-redF-plain from Micromod Partikeltechnologie GmbH, Rostock-Warnemuende, Germany) have an average diameter of 100 μm. Fig. 3 provides representative closed-loop control against 4 flow rates. The disturbance force exerted on the microparticle due to the flow is not compensated ($\widehat{\mathbf{d}}(\dot{\mathbf{P}}) = 0$). At flow rates of 4 ml.hr^{-1} and 35 ml.hr^{-1} the speed of the controlled microparticle is calculated to be 150 μm.s^{-1} and 125 μm.s^{-1}, respectively, whereas the maximum error in the steady-state is 10 μm and 65 μm, respectively. This representative experimental result indicates that the PD control system cannot compensate the disturbance force due to the time-varying flow inside the channel. We repeat this experiment 5 times at each flow rate, and the average speed and maximum position tracking error are calculated to be 150$\pm$4.42 μm.s^{-1} and 10 μm, 145$\pm$0.82 μm.s^{-1} and 47 μm, 135$\pm$4.62 μm.s^{-1} and 55 μm, and 312.5$\pm$4.88 μm/s and 64 μm, at flow rates of 4 ml.hr^{-1}, 6 ml.hr^{-1}, 17 ml.hr^{-1}, and 35 ml.hr^{-1}, respectively. *Please refer to the accompanying video that demonstrates the motion control of a microparticle*

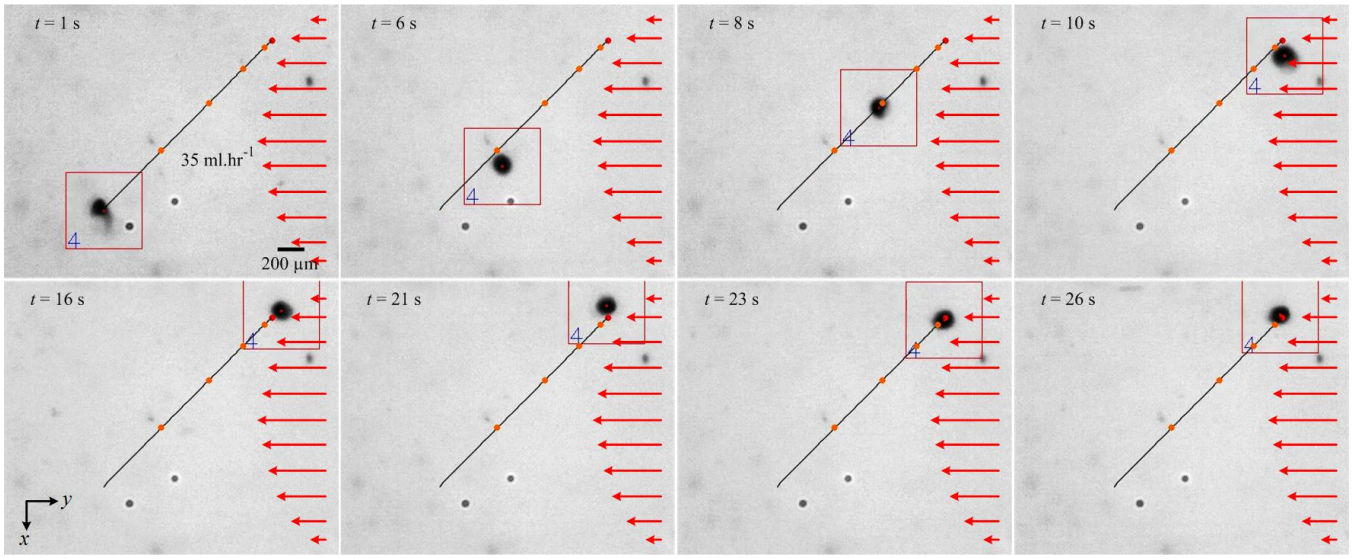

Fig. 5. A representative closed-loop motion control of a paramagnetic microparticle inside a microfluidic channel. The microparticle is controlled against flow rate of 35 ml.hr^{-1} using control law (9). The microparticle moves towards the reference position along a path (black line) at an average speed of 110 μm.s^{-1}. The orange points represent waypoints along the path, whereas the reference position is indicated using a small red circle. The red square is assigned by our feature tracking algorithm and provides the position of the microparticles. The flow lines are indicated using the red arrows. *Please refer to the accompanying video that demonstrates the closed-loop motion control against time-varying flow.*

without disturbance compensation.

Control law (9) is implemented at the mentioned flow rates, as shown in Fig. 4. We observe that the characteristic of the closed-loop control system are improved in the transient- and the steady-state. At flow rates of 4 ml.hr^{-1} and 35 ml.hr^{-1}, the average speed of the microparticle are calculated to be 300 μm.s^{-1} and 370 μm.s^{-1}, respectively, whereas the maximum errors are calculated to be 5 μm and 18 μm, respectively. We repeat this experiment 5 times at each flow rate, and the average speed and maximum position tracking error are calculated to be 304$\pm$5.4 μm.s^{-1} and 5 μm, 322$\pm$0.7 μm.s^{-1} and 14 μm, 350$\pm$3.5 μm/s and 15 μm, and 375$\pm$3.4 μm.s^{-1} and 18 μm, at flow rates of 4 ml.hr^{-1}, 6 ml.hr^{-1}, 17 ml.hr^{-1}, and 35 ml.hr^{-1}, respectively. A representative motion control against flow rate of 35 ml.hr^{-1} is provided in Fig. 5. The microparticles is pulled controllably along a path (black line) and waypoints (orange points) towards the reference position (small red circle). The microparticle is controlled at an average speed of 110 μm.s^{-1} and the maximum steady-state error is calculated to be 5 μm. *Please refer to the accompanying video that demonstrates the motion control of a microparticle with disturbance compensation.*

The PD control system without and with disturbance compensation are compared in Fig. 6. At flow rate of 4 ml.hr^{-1}, the position error in the steady-state is almost similar. However, a significant improvement is achieved by the PD control with disturbance compensation as we increase the flow rate, as opposed to the PD control without compensation. The average steady-state error is decreased by 81.4%, 70.2%, and 70.3% for flow rates of 6 ml.hr^{-1}, 17 ml.hr^{-1}, and 35 ml.hr^{-1}, respectively. The speed of the controlled microparticle decreases linearly with the increasing flow rate.

IV. CONCLUSIONS AND FUTURE WORK

This study demonstrates experimentally the ability to controllably navigate paramagnetic microparticles against and along time-varying flow rates. A control system is designed based on disturbance estimation and compensation. The drag force and force due to flow are modeled as time-varying disturbance force. This model is used in the design of a disturbance force observer that is used as an inner-loop (positive feedback) of the closed-loop control system. This control strategy enables localization of microparticles against flow rate of 35 ml.hr^{-1}, with average error of 18 μm, whereas a magnetic-based control without disturbance compensation achieves average error of 54 μm in the steady-state.

As part of future studies, the microparticles and nanoparticles will be coated with a chemotherapeutic agent and selective motion control towards cancer cells will be achieved *in vitro* [24]. This future study is essential to understand some of the challenges that still remain to translate the magnetic-based control of microagents into *in vivo* applications. In addition, our electromagnetic system will be redesigned to generate greater magnetic field gradient than 220 mT.mm^{-1}. The field gradient is necessary to study flow rates similar to those used in animal experimentation. Our system will also be adapted to integrate a microforce sensing probe and an ultrasound imaging modality [25] to measure the force due to the time-varying flow and provide feedback to the control system, respectively. We will also achieve motion control of microparticles against the flowing streams of a fluid inside catheter segments using an electromagnetic system with an open-configuration [26], [27], [28].

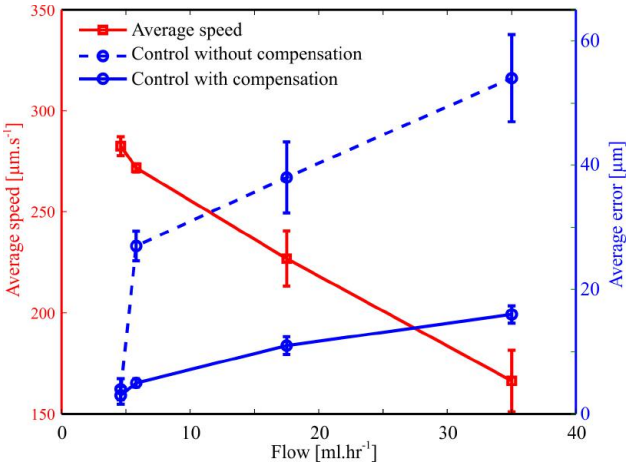

Fig. 6. Average speed and steady-state error of the controlled microparticles versus the flow rate inside the microfluidic channel. The average speed and error are calculated using 5 closed-loop control trials at each flow rate for proportional-derivative control system without and with disturbance compensation. The magnetic field gradient exerted on the microparticle cannot overcome flow rates greater than 35 ml.hr^{-1}. The disturbance compensation enables a reduction in the position error of 81.4%, 70.2%, and 70.3% for flow rates of 6 ml.hr^{-1}, 17 ml.hr^{-1}, and 35 ml.hr^{-1}, respectively.

V. ACKNOWLEDGMENTS

The authors would like to thank Dr. Rasha El-Nashar and Dr. Mohamed Serry for assistance with the experimental work.

REFERENCES

[1] Q. A. Pankhurst, J. Connolly, S. K. Jones, and J. Dobson, "Applications of magnetic nanoparticles in biomedicine," *Journal of Physics*, vol. 36, no. 13, pp. 167-181, June 2003.

[2] B. J. Nelson, I. K. Kaliakatsos, and J. J. Abbott, "Microrobots for minimally invasive medicine," *Annual Review of Biomedical Engineering*, vol. 12, pp. 55-85, April 2010.

[3] K. Belharet, D. Folio, and A. Ferreira, "Simulation and planning of a magnetically actuated microrobot navigating in the arteries," *IEEE Transactions on Biomedical Engineering*, vol. 60, no. 4, pp. 994–1001, April 2013.

[4] R. Sinha, G. J. Kim, S. Nie, and D. M. Shin, "Nanotechnology in cancer therapeutics: bioconjugated nanoparticles for drug delivery," *Molecular Cancer Therapeutics*, Vol. 5, no. 8, pp. 1909-1917, August 2006.

[5] K. Youakim, M. Ehab O. Hatem, S. Misra, and I. S. M. Khalil, "Paramagnetic microparticles sliding on a surface: characterization and closed-loop motion control," *Proceedings of the IEEE International Conference on Robotics and Automation (ICRA)*, pp. 4068-4073, Seattle, USA, May 2015.

[6] J. Weizenecker, B. Gleich, J. Rahmer, H. Dahnke, and J. Borgert, "Three-dimensional real-time in *vivo* magnetic particle imaging," *Physics in Medicine and Biology*, vol. 54, no. 5, pp. 1-10, March 2009.

[7] A. S. Lübbe, C. Bergemann, J. Brock, and D. G. McClure, "Physiological aspects in magnetic drug-targeting," *Journal of Magnetism and Magnetic Materials*, vol. 194, no. 1-3, pp. 149-155, April 1999.

[8] J. Wang and W. Gao, "Nano/Microscale motors: biomedical opportunities and challenges," *ACS Nano*, vol. 6, no. 7, pp. 5745-5751, July 2012.

[9] S. Sanchez, A. A. Solovev, S. M. Harazim, and O. G. Schmidt, "Microrobots swimming in the flowing streams of microfluidic channels," *Journal of the American Chemical Society*, vol. 133, no. 4, pp. 701-703, December 2010.

[10] I. S. M. Khalil, V. Magdanz, S. Sanchez, O. G. Schmidt, and S. Misra, "The control of self-propelled microjets inside a microchannel with time-varying flow rates," *IEEE Transactions on Robotics*, vol. 30, no. 1, pp. 49-58, February 2013.

[11] A. Nacev, C. Beni, O. Bruno, and B. Shapiro, "Magnetic nanoparticle transport within flowing blood and into surrounding tissue, *Nanomedicine*, vol. 5, no. 9, pp. 1459-1466, November 2010.

[12] I. S. M. Khalil, L. Abelmann, and S. Misra, "Magnetic-based motion control of paramagnetic microparticles with disturbance compensation," *IEEE Transactions on Magnetics*, vol. 50, no. 10, October 2010.

[13] I. S. M. Khalil, R. M. P. Metz, B. A. Reefman, and S. Misra, "Magnetic-Based minimum input motion control of paramagnetic microparticles in three-dimensional space," *Proceedings of the IEEE/RSJ International Conference of Robotics and Systems (IROS)*, pp. 2053-2058, Tokyo, Japan, November 2013.

[14] Z. J. Yang, H. Tsubakihara, S. Kanae, K. Wada, and C. Yi. Su, "A novel robust nonlinear motion controller with disturbance observer," *IEEE Transactions on Control Systems Technology*, vol. 16, no. 1, pp. 137-147, January 2008.

[15] Y. Choi, K. Yang, W. K. Chung, H. R. Kim, and I. H. Suh, "On the robustness and performance of disturbance observers for second-order systems," *IEEE Transactions on Automatic Control*, vol. 48, no. 2, pp. 315-320, February 2003.

[16] S. Katsura, Y. Matsumoto, and K. Ohnishi, "Modeling of force sensing and validation of disturbance observer for force control," *IEEE Transactions on Industrial Electronics*, vol. 54, no. 1, pp. 530-538, February 2007.

[17] I. S. M. Khalil, H. Abass, M. Shoukry, A. Klingner, R. M. El-Nashar, M. Serry, and S. Misra, "Robust and optimal control of magnetic microparticles inside fluidic channels with time-varying flow rates," *International Journal of Advanced Robotic Systems*, vol. 13 (DOI: dx.doi.org/10.5772/63517). *In Press*

[18] M. P. Kummer, J. J. Abbott, B. E. Kartochvil, R. Borer, A. Sengul, and B. J. Nelson, "OctoMag: an electromagnetic system for 5-DOF wireless micromanipulation," *IEEE Transactions on Robotics*, vol. 26, no. 6, pp. 1006-1017, December 2010.

[19] B. Esteban, J.-R. Riba, G. Baquero, A. Rius, and R. Puig, "Temperature dependence of density and viscosity of vegetable oils," *Biomass and bioenergy*, vol. 42, pp. 164-171, July 2012.

[20] B. R. Munson, W. W. Huebsch, and A. P. Rothmayer, "Fundamentals of fluid mechanics," Wiley, 2005.

[21] I. S. M. Khalil, R. M. P. Metz, L. Abelmann, and S. Misra, "Interaction force estimation during manipulation of microparticles," *Proceedings of the IEEE/RSJ International Conference of Robotics and Systems (IROS)*, pp. 950–956, Vilamoura, Algarve, Portugal, October 2012.

[22] I. S. M. Khalil, M. P. Pichel, L. Abelmann, and S. Misra, "Closed-loop control of magnetotactic bacteria," in *The International Journal of Robotics Research*, vol. 32, no. 6, pp. 637-649, May 2013.

[23] I. S. M. Khalil, K. Youakim, A. Sánchez, S. Misra "*Magnetic-based motion control of sperm-shaped microrobots using weak oscillating magnetic fields*", *Proceedings of the IEEE International Conference of Robotics and Systems (IROS)*, pp. 4686-4691, Chicago, USA, September 2014.

[24] I. S. M. Khalil, I. E. O. Gomaa, R. M. Abdel-Kader and S. Misra, "Magnetic-Based contact and non-contact manipulation of cell mock-ups and MCF-7 human breast cancer cells," *Smart Drug Delivery System*, Intech, ch. 9, pp. 219-235, February 2016.

[25] I. S. M. Khalil, P. Ferreira, R. Eleutério, C. L. de Korte, and S. Misra, "Magnetic-based closed-loop control of paramagnetic microparticles using ultrasound feedback," *Proceedings of the IEEE International Conference on Robotics and Automation (ICRA)*, pp. 3807-3812, Hong Kong, June 2014.

[26] A. W. Mahoney, J. C. Sarrazin, E. Bamberg, and J. J. Abbott, "Velocity control with gravity compensation for magnetic helical microswimmers," *Advanced Robotics*, vol. 28, no. 8, pp. 1007-1028, April 2012.

[27] I. S. M. Khalil, B. E. Wissa, B. G. Salama, and S. Stramigioli, "Wireless motion control of paramagnetic microparticles using a magnetic-based robotic system with an open-configuration," *Proceedings of the International Conference on Manipulation, Manufacturing and Measurement on the Nanoscale (3M Nano)*, Changchun, China, pp. 190-196, October 2015.